RSC Applied Interfaces

ROYAL SOCIETY OF CHEMISTRY

PAPER

View Article Online
View Journal | View Issue

Check for updates

Cite this: *RSC Appl. Interfaces*, 2025, **2**, 1041

One-pot synthesis of necklace-like MOF@CNTs: a universal strategy for enhancing molecular separation performance in mixed-matrix membranes†

Xuemeng Jia, ‡*[ab] Zhenting Song,‡[a] Qiaomei Li,[a] Jiacheng Huang,[a] Xiaowen Zhai,[a] Lei Tian,[c] Jinlou Li,[d] Zhihua Qiao,[e] Yuhui Luo *[ab] and Dongen Zhang[ab]

Metal–organic frameworks (MOFs) are usually employed as fillers within a polymer matrix to fabricate mixed matrix membranes (MMMs). However, the aggregation of MOFs, particularly at the nanoscale, frequently leads to defects at the filler–polymer interface, making it difficult to form continuous molecular transport channels. Here, a series of necklace-like MOF@carbon nanotubes (CNTs) were synthesized using a straightforward one-pot technique. Specifically, CNTs as a "lead wire" with substantial aspect ratios were first used to induce the self-assembly growth of MOFs as "beads" along the CNTs' longitudinal axis, for the preparation of necklace-like MOF@CNTs. Subsequently, necklace-like MOF@CNTs MMMs were obtained by interfacial polymerization or solvent evaporation. MOF@CNTs have good dispersibility in the polymer matrix and the MOFs within the necklace are in close contact and effectively link the MOF window to create micrometer-scale continuous molecular transport channels that can improve the separation performance of MMMs. For ZIF-90/PA mixed matrix nanofiltration membranes, the water permeability of M-ZIF-90@CNTs (27.15 L m^{-2} h^{-1} bar^{-1}) is greater than that of M-0 (8.11 L m^{-2} h^{-1} bar^{-1}). Furthermore, the dye rejection efficiency has been increased from 96.60% of M-0 to 99.55% of M-ZIF-90@CNTs and the rejection of NaCl remains relatively low across all nanofiltration membranes, at less than 10%, which has significant advantages in the field of dye/salt separation. For ZIF-90/PSf mixed matrix gas separation membranes, MPSf-ZIF-90@CNTs also exhibit remarkable CO_2/N_2 separation selectivity. Importantly, the proposed strategy for preparing necklace-like MOF@CNTs is universally applicable, and can be easily extended to other MOFs, such as ZIF-8, MOF-801, UiO-66, and UiO-66-NH_2, representing a universal strategy for constructing necklace-like MOF@CNTs structures.

Received 26th January 2025,
Accepted 14th April 2025

DOI: 10.1039/d5lf00016e

rsc.li/RSCApplInter

1. Introduction

Membrane separation, as an emerging type of separation technology, possesses advantages such as high efficiency, energy conservation, environmental friendliness, and a smaller footprint.[1–4] In recent years, it has become one of the research hotspots in the field of chemical industry separation. Mixed matrix membranes (MMMs) combining the mechanical properties, processability and cost-effectiveness of polymers with the permeability and selectivity of fillers, have attracted the attention in food,[5] medicine,[6] environmental protection,[7] chemical industry,[8] energy,[9] water treatment[10] and other fields.[11,12] Metal–organic frameworks (MOFs) are often used as fillers for the preparation of MMMs, owing to their ultra-high specific surface area, a wide array of designable structural types, and the ability to adjust their chemical functionalities.[13–15] However, the agglomeration phenomenon between MOF nanoparticles can lead to filler–polymer interface defects and difficulty in forming continuous molecular transport channels, thereby affecting the separation efficiency of MMMs.[16,17] Therefore, how to improve the dispersibility of MOFs in the polymer, and

[a] *School of Environmental and Chemical Engineering, Jiangsu Key Laboratory of Function Control Technology for Advanced Materials, Jiangsu Ocean University, Lianyungang, Jiangsu, 222005, China. E-mail: Jiaxm@jou.edu.cn, luoyh@jou.edu.cn*
[b] *Jiangsu Institute of Marine Resources Development, Lianyungang, Jiangsu, 222005, China*
[c] *The Institute of Seawater Desalination and Multipurpose Utilization, MNR (Tianjin), Tianjin, 300192, China*
[d] *Lianyungang Petrochemical Co., Ltd., Lianyungang, Jiangsu, 222065, China*
[e] *State key laboratory of separation membranes and membrane processes, Tiangong University, Tianjin, 300387, China*

† Electronic supplementary information (ESI) available. See DOI: https://doi.org/10.1039/d5lf00016e

‡ These authors contributed equally to this work.

construct suitable continuous molecular transport channels to achieve rapid selective passage of guest molecules in MMMs are the keys to obtaining high-performance MOF-based MMMs.

The precise arrangement of MOFs in a polymer matrix is crucial for improving dispersibility and establishing continuous molecular transport channels. To date, it has been extensively reported that various arrangements of MOF fillers have been precisely designed to overcome MOF aggregation in polymer membranes. Researchers have concentrated on the design of the MOF shape or surface functionalization of MOFs to improve dispersion. Aydin Ozcan *et al.*[18] demonstrated that the nanostructure of interfacial pores plays a key role in optimum molecular transport. The prototypical ultrasmall pore AlFFIVE-1-Ni MOF was assembled with the polymer PIM-1 and the oriented AlFFIVE-1-Ni MOF/PIM-1 MMMOF membranes were prepared. The findings indicated that the CO_2 gas separation performance of the oriented MOF nanosheets was greatly improved by their uniform distribution in the polymer matrix. Fei *et al.*[19] introduced the self-assembly of superhydrophilic amino-acid-based Zr-MOF microcrystals (MIP-202(Zr)) into nanoporous membranes utilizing graphene oxide (GO) as a two-dimensional (2D) nano-surfactant. The GO/MIP-202(Zr) membrane exhibited a uniform distribution of MOF microcrystals and the formation of two-dimensional/three-dimensional (2D/3D) hybrid nanochannels. Consequently, the water separation performance of the GO/MIP-202(Zr) membrane surpassed that of numerous other GO/MOF composite membranes. Nevertheless, although these approaches have improved MOF dispersion in polymer matrices to some extent, modification processes remain highly contingent on MOF surface chemistry, demanding tailored strategies for different systems. Moreover, discrete MOF particles cannot form interconnected molecular pathways, making it challenging to achieve highly continuous transport channels in MMMs.

Potentially, several studies have suggested that necklace-like MOF structures, where MOF particles serve as "beads" aligned along the longitudinal axis direction of high-aspect-ratio nanotubes or nanowires ("lead wires"), are a viable alternative. Highly continuous MOF sequences are in close contact and effectively link the MOF window to create a relatively continuous molecular pathway, and the MOFs maintain nanoscale dimensions with uniform and stable dispersion in the polymer membrane matrix. Xu *et al.*[20] developed a unique necklace-like zeolitic imidazolate framework (ZIF-8) embedded with polypyrrole (PPy) nanotubes, denoted as ZIF-8@PPy. The inclusion of necklace-like ZIF-8 throughout a PDMS matrix resulted in the formation of micron-sized, ultrahighly continuous multiple guest molecule transport channels and significantly reduced the voids and defects caused by agglomeration, which are ideal for pervaporation separation. In the case of 1 wt% *n*-butanol aqueous solutions, the resulting MMMs containing 20 wt% ZIF-8@PPy exhibited a remarkable enhancement in the separation factor, increasing from 36.4 to 70.2. Concurrently, the total flux was also boosted, increasing from 312.4 to 564.8 g m^{-2} h^{-1}. Despite all of these, the current synthesis of necklace-like MOFs remains cumbersome and lacks a universal preparation approach, hindering their rational application in polymer matrices. If a universal and simple strategy for preparing necklace-like MOFs is developed to improve the dispersion of MOFs in MMMs, and constructing highly continuous guest molecule transport channels by reasonable loading, it is expected to achieve high-performance MOF-based MMMs.

Carbon nanotubes (CNTs), a one-dimensional nanomaterial with excellent aspect ratios, have a tubular structure composed of interconnected layers of carbon atoms coiled together. CNTs have high elastic modulus and tensile strength, excellent mechanical properties, good conductivity and thermal conductivity, which shows a great research value.[21–24] In addition, the surface of CNTs contains defects and is easily functionalized.[25,26] Combining CNTs with other materials to form new composite materials to enhance material properties and multifunctional applications is a further research direction.

In this work, a simple one-pot synthesis strategy to prepare necklace-like MOF@CNTs has been innovatively proposed to solve the problem of MOF aggregation in polymers and difficulty in forming highly continuous molecular transport channels in MMMs. Detailly, CNTs, metal ions, and ligands were added to the flask, and a necklace-like structure MOF@CNTs with good crystallinity was prepared by utilizing the defects or functional groups on the surface of CNTs as nucleation sites, enabling the directional self-assembly of MOFs along the CNT longitudinal axis. Afterward, necklace-like MOF@CNTs MMMs were prepared using MOF@CNTs as fillers (Scheme 1). This preparation strategy not only allows for effective and stable dispersion of nanoscale MOFs in polymers, but also enables efficient docking of MOF windows to form micrometer-scale continuous multi guest-molecular transport channels without changing the internal structure of MOFs to enhance the separation performance of MMMs. Significantly, the proposed one-pot synthesis approach is universally applicable, which can be easily extended to different types of MOFs, such as ZIF-90, ZIF-8, MOF-801, UiO-66, and UiO-66-

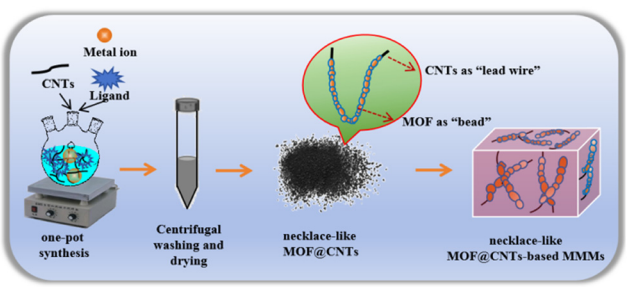

Scheme 1 Schematic illustration for the process of preparing necklace-like MOF@CNTs and MOF@CNTs-based MMMs.

NH_2, representing a universal strategy for constructing necklace-like MOF@CNTs structures.

2. Experimental section

2.1 Materials

All the reagents and solvents are commercially available without further purification. Multi-walled carbon nanotubes (CNTs, >95%) and carboxylated multi-walled carbon nanotubes (c-CNTs, >95%) were purchased from Aladdin. Zinc nitrate hexahydrate, ($Zn(NO_3)_2{\cdot}6H_2O$, 99%), zirconium(IV) chlorideanhydrous ($ZrCl_4$, 99.99%) and zirconyl chloride octahydrate ($ZrOCl_2{\cdot}8H_2O$, 98%) were obtained from Sigma Aldrich. 2-Imidazolecarboxaldehyde (2-ICA, 98%), 2-methylimidazole (2-mIm, 99%), fumaric acid (99%), terephthalic acid (H_2BDC, 99%), 2-aminoterephthalic acid (98%), piperazine (PIP, 99%), 1,3,5-benzenetricarbonyl trichloride (TMC, 99%), and triethylamine (99%) were purchased from InnoChem. Acetic acid (AR), *N*,*N*-dimethylformamide (DMF, AR), methanol (AR), chloroform ($CHCl_3$, AR), formic acid (AR), and hexane (AR) was purchased from National Guoyao Group Chemical Reagent Co., Ltd. Polysulfone (PSf, WM = 50 000) ultrafiltration membrane was purchased from RisingSun Membrane Technology (Beijing) Co., Ltd. Polysulfone (PSf, s6010) was purchased from Jiangsu SuoEr Engineering Plastics Co., Ltd. Sodium chloride (NaCl) and congo red (CR) were purchased from Sinopharm Chemical Reagents Co., Ltd. Deionized (DI) water was deionized by Millipore Direct-Q apparatus.

2.2 Preparation of necklace-like MOF@CNTs

2.2.1 Preparation of necklace-like ZIF-90@CNTs and ZIF-90@c-CNTs. Taking necklace-like ZIF-90@CNTs as a typical example, the one-pot synthesis steps are as follows: the amount of CNTs (0.03 g, 0.05 g, 0.08 g, 0.1 g) were added into 100 mL of DMF, and uniformly dispersed by ultrasonic treatment for 50 min. Then, ICA (0.48 g, 5 mmol), $Zn(NO_3)_2{\cdot}6H_2O$ (0.287 g, 40 mmol) and triethylamine (3 mL) were sequentially dissolved in the above solution. Subsequently, the solution was evenly stirred at 80 °C for 8 h to form ZIF-90@CNTs. Finally, the powder was collected by centrifuging, washing with DMF and methanol for several times, and drying at 50 °C for 12 h in vacuum. Different modified ZIF-90@CNTs were fabricated by adjusting the corresponding weight of CNTs and named as ZIF-90@CNTs-0.03, ZIF-90@CNTs-0.05, ZIF-90@CNTs-0.08 and ZIF-90@CNTs-0.1, respectively.

In order to investigate the effects of surface functional groups and aspect ratio of CNTs on the synthesis of necklace-like MOF@CNTs, c-CNTs were used instead of CNTs, and the other steps were the same as those of ZIF-90@CNTs to prepare ZIF-90@c-CNTs.

Further, to verify that the strategy for preparing ZIF-90 is universal and general, other MOFs such as ZIF-8, MOF-801, UiO-66, and UiO-66-NH_2 were also used to fabricate MOF@CNTs as well as MOF@c-CNTs.

2.2.2 Preparation of necklace-like ZIF-8@CNTs and ZIF-8@c-CNTs. CNTs (0.05 g) were added into 30 mL of DMF, and uniformly dispersed by ultrasonic treatment for 50 min. Then, 2-mIm (1.31 g, 16 mmol) and $Zn(NO_3)_2{\cdot}6H_2O$ (0.595 g, 2 mmol) were dissolved into the above solutions, respectively, and blended well by stirring at room temperature for 24 h to form the ZIF-8@CNTs solution. Finally, the powder was collected by centrifuging, washing with methanol for several times, and drying at 80 °C for 12 h in vacuum.

ZIF-8@c-CNTs was synthesized in the same way as ZIF-8@CNTs, except that CNTs were replaced by c-CNTs.

2.2.3 Preparation of necklace-like MOF-801@CNTs and MOF-801@c-CNTs. Similarly, CNTs (0.05 g) were added into the mixed solution of DMF (40 mL) and formic acid (14 mL), and uniformly dispersed by ultrasonic treatment for 50 min. Then, fumaric acid (0.58 g, 5 mmol), $ZrOCl_2{\cdot}8H_2O$ (1.61 g, 5 mmol) were dissolved into the above solutions, respectively, and blended well by kept stirring at 130 °C for 6 h to form MOF-801@CNTs solution. Finally, the powder was collected by centrifuging, washing with DMF and methanol for several times, and drying at 150 °C for 24 h in vacuum.

MOF-801@c-CNTs was synthesized in the same way as MOF-801@CNTs, except that CNTs were replaced by c-CNTs.

2.2.4 Preparation of necklace-like UiO-66@CNTs and UiO-66@c-CNTs. Similarly, CNTs (0.05 g) were added into 50 mL of DMF, and uniformly dispersed by ultrasonic treatment for 50 min. Then, H_2BDC (0.166 g, 1 mmol), $ZrCl_4$ (0.233 g, 1 mmol) and acetic acid (6 mL) were dissolved into the above solutions, respectively, and blended well by kept stirring at 120 °C for 6 h to form UiO-66@CNTs solution. Finally, the powder was collected by centrifuging, washing with methanol for several times, and drying at 100 °C for 12 h in vacuum.

UiO-66@c-CNTs was synthesized in the same way as UiO-66@CNTs, except that CNTs were replaced by c-CNTs.

2.2.5 Preparation of necklace-like UiO-66-NH_2@CNTs and UiO-66-NH_2@c-CNTs. Similarly, CNTs (0.05 g) were added into 50 mL of DMF, and uniformly dispersed by ultrasonic treatment for 50 min. Then, 2-aminoterephthalic acid (0.225 g, 1.2 mmol), $ZrCl_4$ (0.288 g, 1.2 mmol) and acetic acid (9 mL) were dissolved into the above solutions, respectively, and blended well by kept stirring at 120 °C for 24 h to form UiO-66@CNTs solution. Finally, the powder was collected by centrifuging, washing with methanol for several times, and drying at 100 °C for 12 h in vacuum.

UiO-66-NH_2@c-CNTs was synthesized in the same way as UiO-66-NH_2@CNTs, except that CNTs were replaced by c-CNTs.

2.3 Preparation of necklace-like MOF@CNTs mixed matrix membranes

2.3.1 Preparation of necklace-like MOF@CNTs nanofiltration membranes. The nanofiltration membranes based on ZIF-90 were fabricated through interface polymerization (IP), following the literature procedure with minor modifications.[27] Initially, the aqueous phase

consisting of 0.2 wt% PIP and the organic phase containing 0.15 wt% TMC in *n*-hexane were prepared. The fillers (ZIF-90, ZIF-90@CNTs or ZIF-90@c-CNTs) were added into the aqueous phase at a concentration of 0.02 g L^{-1}. Subsequently, 30 mL of the aqueous phase was uniformly distributed on the PSf ultrafiltration membrane substrate surface by vacuum filtration. Any excess aqueous phase was removed by suction with absorbent paper from the back of the PSf substrate, and 10 mL of the organic phase was then applied to completely cover the membrane surface for interface polymerization. After 30 s, the excess organic phase was discarded, and the resulting mixed matrix membranes (MMMs) were heated in an oven at 60 °C to ensure complete reaction. Finally, the prepared MMMs were preserved in RO water for further processing (Scheme 2). Different nanofiltration membranes were fabricated by adjusting fillers and named as M-0, M-ZIF-90, M-ZIF-90@CNTs, and M-ZIF-90@c-CNTs, respectively.

2.3.2 Preparation of necklace-like MOF@CNTs gas separation membranes. In a typical approach, the ZIF-90-based MMMs were synthesized using a solvent evaporation technology, as depicted in Scheme 3. First, PSf powders were dissolved into $CHCl_3$ solution and blended well by continuous stirring at room temperature for 12 h to yield the 10 wt% homogeneous polymer solution. Subsequently, 10 wt% fillers (ZIF-90, ZIF-90@CNTs or ZIF-90@c-CNTs) relative to the PSf mass were dispersed in 10 mL of the above solution, followed by stiring vigorously for 48 h to achieve a uniform suspension. Then, the solution was allowed to stand for 6 hours to remove any bubbles before being casted on a glass plate using a 200 μm scraping knife. After that, the solvent is slowly evaporated at 25 °C. Finally, the freshly prepared MMMs were vacuum dried at 40 °C for another 6 hours before use.

2.4 Characterization

The powder and membranes were characterized by X-ray diffraction (XRD, D2 Discover, Bruker, Germany) within a 2θ range of 3–40° and Fourier transform infrared (FTIR) spectroscopy with a Vector 22 spectrometer (Bruker Daltonics Inc., Germany). The morphology of the gold-plated samples was observed *via* a Field-emission scanning electron microscope (SEM, Hitachi S-4800, Japan). N_2 adsorption–desorption isotherms at 77 K were recorded using a Micromeritics ASAP 2020 Plus HD88 instrument and the pore distribution data were calculated employing density functional theory (NLDFT).

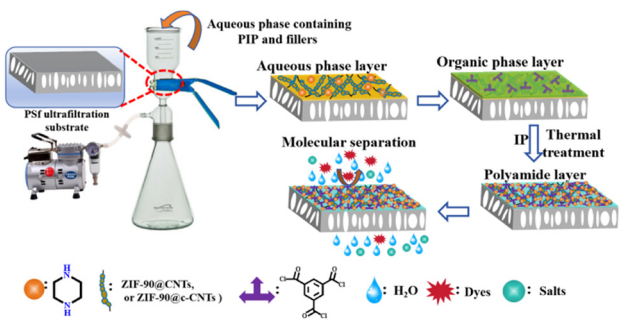

Scheme 2 Schematic illustration for the process of preparing MOF@CNTs-based nanofiltration membranes for molecular separation.

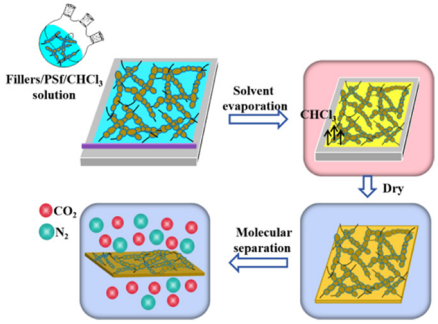

Scheme 3 Schematic illustration for the process of preparing MOF@CNTs-based gas separation membranes for molecular separation.

2.5 Molecular separation performance of MMMs

(1) Dye/salt separation performance. Filtration and the rejection performance of the nanofiltration membranes were evaluated through cross-flow experiments as previously described with slight modifications.[28]

All filtration studies were conducted at room temperature under a transmembrane pressure of 3 bar using a membrane low-pressure evaluator. The effective membrane area was 7.065 cm^2. Prior to testing, the membrane was pre-pressurized at 3 bar for at least 30 minutes to achieve a stable state. The pure water permeability (P, in units of Lm^{-2} h^{-1} bar^{-1}) was calculated using the following equation:

$$P = \frac{V}{A \times \Delta t \times \Delta P} \quad (1)$$

where V (L) represents the volume of the collected permeate, A (m^2) represents the effective membrane area, Δt (h) represents the permeation duration, and ΔP (bar) represents the trans-membrane pressure.

To evaluate the separation performance of the nanofiltration membranes, Congo red (CR) dispersed in pure water at a concentration of 100 ppm and NaCl dispersed in pure water at a concentration of 1000 ppm are used as feed solutions. The rejection (R, %) is obtained using the following formula:

$$R = \left(1 - \frac{C_p}{C_f}\right) \times 100\% \quad (2)$$

where C_p and C_f are the permeate and feed solute concentrations, respectively.

(2) Gas separation performance. Gas separation performance of the membranes was assessed using gas permeance test equipment, following the methodologies established in our earlier work.[29]

The gas permeability (P) can be calculated by the following equation:

$$P = R \times l \quad (3)$$

where P is the gas permeability (in units of barrer, 1 barrer = 10^{-10} cm^3 (STP) cm cm^{-2} s^{-1} $cmHg^{-1}$ = 3.35×10^{-16} mol m m^{-2} s^{-1} Pa^{-1}), R is the gas permeance (in units of GPU, 1 GPU = 10^{-6} cm^3 (STP) cm^{-2} s^{-1} $cmHg^{-1}$ = 3.35×10^{-10} mol m^{-2} s^{-1} Pa^{-1}), and l is the thickness of selective layer (in units of μm). Three individual membranes of every type were tested, and the standard deviations are represented by error bars.

The ideal perm-selectivity, $\alpha_{A/B}$, of the membrane for a pair of gases (A and B) is defined as the ratio of the individual gas permeability coefficients:

$$\alpha_{A/B} = \frac{P_A}{P_B} \quad (4)$$

3. Results and discussion

3.1 Characterization of necklace-like MOFs

ZIF-90, which has the same topology as ZIF-8, has not only high stability, but also a micropore size and large specific surface area.[30] Benefiting from the free aldehyde group on the ligand, ZIF-90 has high functionalization potential to form ZIF-90-derived materials with different porosity. Yaghi *et al.*[31] reported the conversion of the free CHO group on ZIF-90 to an alcohol and ethanolamine to an imine to form ZIF-91 and ZIF-92, respectively. Thus, ZIF-90 has great application potential in the fields of water treatment, gas separation, catalysis, *etc.*[32–34]

As a proof of concept, ZIF-90@CNTs was first prepared and characterized. The morphology of ZIF-90 and ZIF-90@CNTs nanoparticles were studied by SEM. As shown in Fig. 1(a1 and a2), ZIF-90 has a nanosphere morphology with a diameter of about 80 nm, and ZIF-90 appears to be in an aggregated state. With the addition of CNTs, the morphology of ZIF-90 changes and gradually transitions to a polyhedral structure morphology. The observed changes in MOF morphology may be attributed to the surface defects or functional groups on the CNTs, which can serve as nucleation centers, chemically coordinating with MOF metal nodes or organic linkers, inducing the initiation of MOF self-assembly growth along the CNTs' longitudinal axis. The incorporation of CNTs may potentially alter the growth kinetics of MOFs, thereby affecting the size and shape of MOFs.[35] To be specific, it can be seen that when the CNTs addition amount is 0.03 g, the shape and size of ZIF-90 is uneven, resulting in partial growth of ZIF-90 in series on the CNTs "lead wire" (Fig. 1(b1 and b2)). At a CNTs loading of 0.05 g, ZIF-90 grow uniformly and densely along the CNTs "lead wire", forming a well-dispersed composite structure (Fig. 1(c1 and c2)). In addition, with the amount of CNTs added further increases, too many CNTs become randomly entangled, and the size of ZIF-90 becomes more uneven that a very small number of ZIF-90 series connected to CNTs (Fig. 1(d1 and d2) and (e1 and e2)).

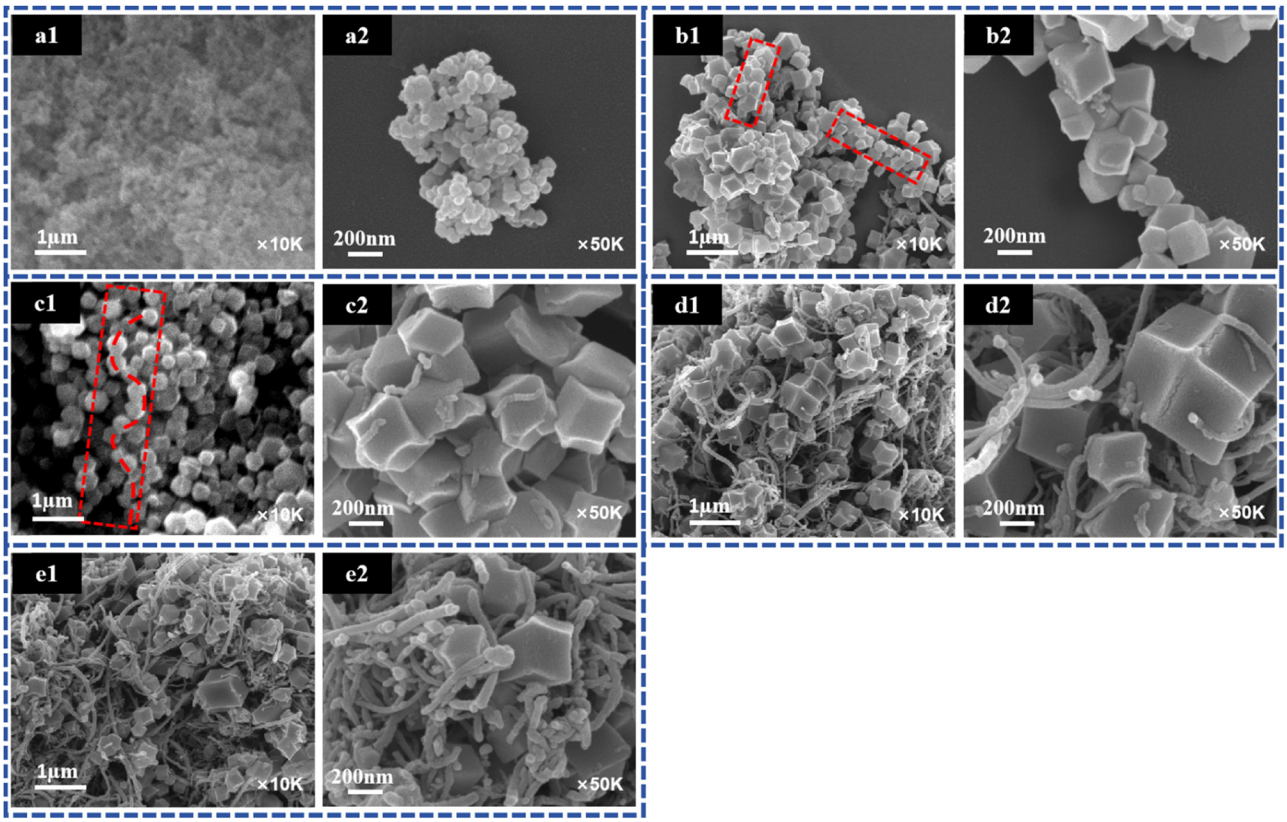

Fig. 1 SEM images of (a1 and a2) ZIF-90, (b1 and b2) ZIF-90@CNTs-0.03, (c1 and c2) ZIF-90@CNTs-0.05, (d1 and d2) ZIF-90@CNTs-0.08, and (e1 and e2) ZIF-90@CNTs-0.1.

As shown in Fig. 1, ZIF-90@CNTs-0.05 presents the best necklace-like structure morphology.

The FTIR spectra of the resultants CNTs, 2-ICA, ZIF-90, and ZIF-90@CNTs are shown in Fig. 2a. Fig. 2a shows the N–H stretching vibration peak of 2-ICA on the imidazole ring at 3110 cm^{-1}. ZIF-90@CNTs powders had the same C═O peak as ZIF-90 at 1690 cm^{-1}, indicating that ZIF-90@CNTs powder was successfully synthesized. The X-ray diffraction (XRD) spectra are shown in Fig. 2b. The diffraction peaks of ZIF-90@CNTs are similar to those of simulated ZIF-90 and prepared ZIF-90, indicating that ZIF-90@CNTs is successfully synthesized, and the crystal structure of ZIF-90 is not affected by the addition of CNTs. The sharp diffraction peak of ZIF-90@CNTs shows ideal purity and high crystallinity.

The specific surface area and pore size distribution of ZIF-90 and ZIF-90@CNTs composites were determined using N_2 adsorption–desorption isotherms at 77 K. As depicted in Fig. 3a, both ZIF-90 and ZIF-90@CNTs exhibit type I isotherms, indicating a typical microporous structure. The Brunauer–Emmett–Teller (BET) surface areas were calculated to be 790.24 $m^2\ g^{-1}$ for ZIF-90 and 770.86 $m^2\ g^{-1}$ for ZIF-90@CNTs. Meanwhile, the total pore volume for ZIF-90@CNTs (0.355 $cm^3\ g^{-1}$) remains nearly identical to that of ZIF-90 (0.352 $cm^3\ g^{-1}$), suggesting that the addition of CNTs does not alter the pore structure of ZIF-90. Additionally, the major pore size distributions for both ZIF-90 and ZIF-90@CNTs are similar, with pore sizes predominantly in the range of 3–6 Å, as illustrated in Fig. 3b.

The water stability of MOFs is crucial for their practical applications.[36,37] In order to explore the influence of the necklace-like MOF@CNTs skeleton structure on water stability, ZIF-90@CNTs was immersed in water with pH = 2 at room temperature, and tested the changes in XRD spectra before and after immersion. Fig. 4a shows the XRD patterns of the original ZIF-90 sample after soaking in water with pH = 2 for 1 day. It can be seen that the characteristic peak intensity of the ZIF-90 has almost no change. Similarly, the XRD patterns of the ZIF-90@CNTs sample after immersion also showed almost no change, maintaining the complete pore structure (Fig. 4b). The above results indicate that ZIF-90@CNTs has excellent water stability and the necklace-like structure has no effect on water stability.

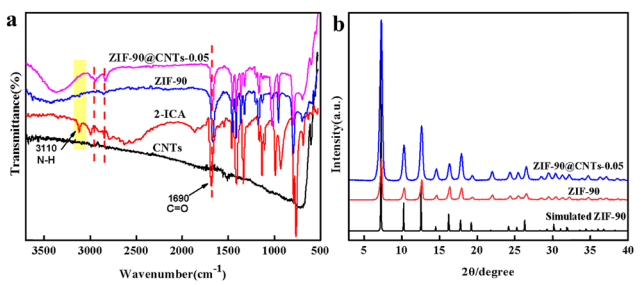

Fig. 2 (a) FTIR spectra of CNTs, 2-ICA, ZIF-90 and ZIF-90@CNTs-0.05, and (b) PXRD patterns of simulated ZIF-90 and the as-synthesized ZIF-90 and ZIF-90@CNTs-0.05.

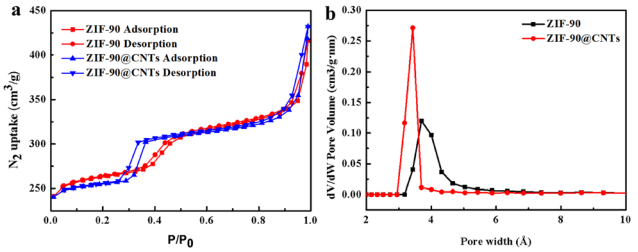

Fig. 3 (a) N_2 adsorption–desorption isotherms at 77 K and (b) pore size distribution data of the as-synthesized ZIF-90 and ZIF-90@CNTs-0.05.

In order to verify the effect of different surface functional groups and different aspect ratios of CNTs on necklace-like MOFs, carboxylated multi-walled carbon nanotubes (c-CNTs) with abundant carboxyl groups on the surface, inner diameter >50 nm and length >10 μm were added instead of CNTs, to prepare ZIF-90@c-CNTs. As shown in Fig. S1a,† ZIF-90@c-CNTs has the same C═N peak at 1670 cm^{-1} as ZIF-90 and ZIF-90@CNTs. The XRD diffraction peaks of ZIF-90@c-CNTs were similar to those of simulated ZIF-90 and purified ZIF-90, indicating the successful synthesis of ZIF-90@c-CNTs and similarly indicating that the crystal structure was not affected by the addition of c-CNTs (Fig. S1b†). The morphology of ZIF-90@c-CNTs is shown in Fig. S2.† ZIF-90 nanoparticles grow closely along the "lead wire" of the c-CNTs, forming a necklace-like ZIF-90@c-CNTs. Furthermore, the BET surface area of ZIF-90@c-CNTs was 770.41 $m^2\ g^{-1}$ and the total pore volume of ZIF-90@CNTs (0.375 $cm^3\ g^{-1}$). Meanwhile, the pore size distribution of ZIF-90@CNTs is 3–6 Å, which is the same trend as ZIF-90@CNTs (Fig. S3†). ZIF-90@c-CNTs also has excellent water stability (Fig. S4†). These above results indicate that ZIF-90 can form necklace-like MOFs with c-CNTs with different surface functional groups and aspect ratios.

To validate the universality of the proposed one-pot synthesis strategy for fabricating necklace-like MOFs through axial growth along CNTs, other MOF materials, such as ZIF-8, MOF-801, UiO-66 and UiO-66-NH_2, were used to fabricate necklace-like MOFs materials. According to the SEM results of these selected MOFs (Fig. 5), as expected, all can form necklace-like MOF@CNTs and MOF@c-CNTs. It is worth noting that the addition of

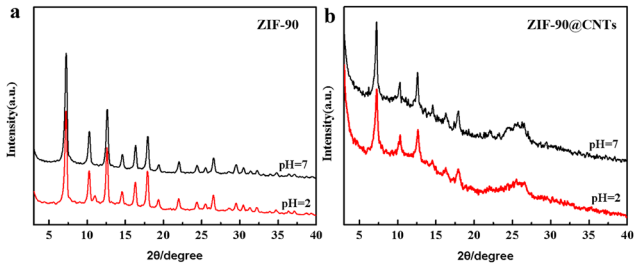

Fig. 4 XRD patterns of (a) ZIF-90 and (b) ZIF-90@CNTs before and after being immersed in pH = 2 water.

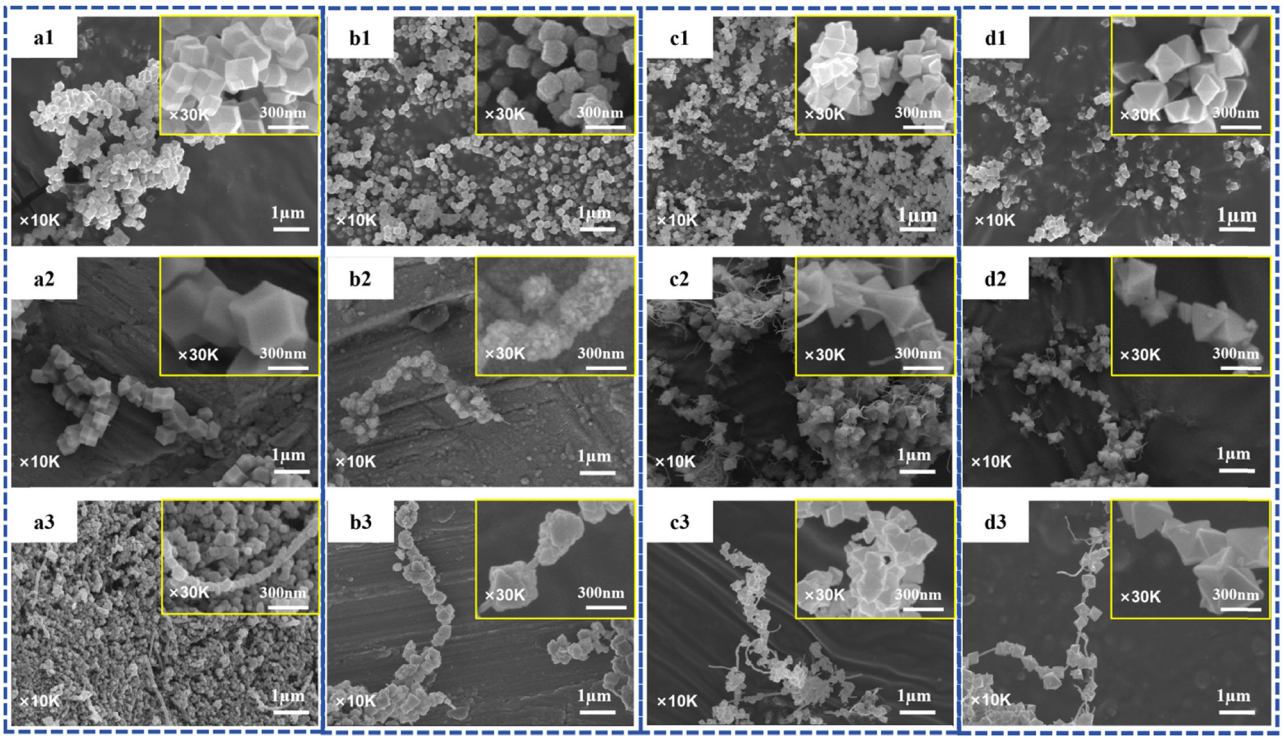

Fig. 5 SEM images of (a1–a3) ZIF-8, ZIF-8@CNTs and ZIF-8@c-CNTs, (b1–b3) MOF-801, MOF-801@CNTs and MOF-801@c-CNTs, (c1–c3) UiO-66, UiO-66@CNTs and UiO-66@c-CNTs, and (d1–d3) UiO-66-NH_2, UiO-66-NH_2@CNTs and UiO-66-NH_2@c-CNTs.

CNTs also changed the size and shape of these selected MOFs. The necklace-like structure effectively connects MOF windows, which can create relatively continuous microscale molecular pathways for MMMs. Correspondingly, the obtained MOF, MOF@CNTs and MOF@c-CNTs are characterized by FT-IR, and XRD. The results show that the synthesis of MOF@CNTs and MOF@c-CNTs were successful (Fig. S5 and S6†).

3.2 Molecular separation performance of ZIF-90@CNTs MMMs

The necklace-like MOFs are in close contact and effectively link the MOF window, creating micrometer-scale continuous multi-guest molecular transport channels to improve the separation performance of MMMs. Polyamide (PA) nanofiltration membrane (M-0) and modified nanofiltration

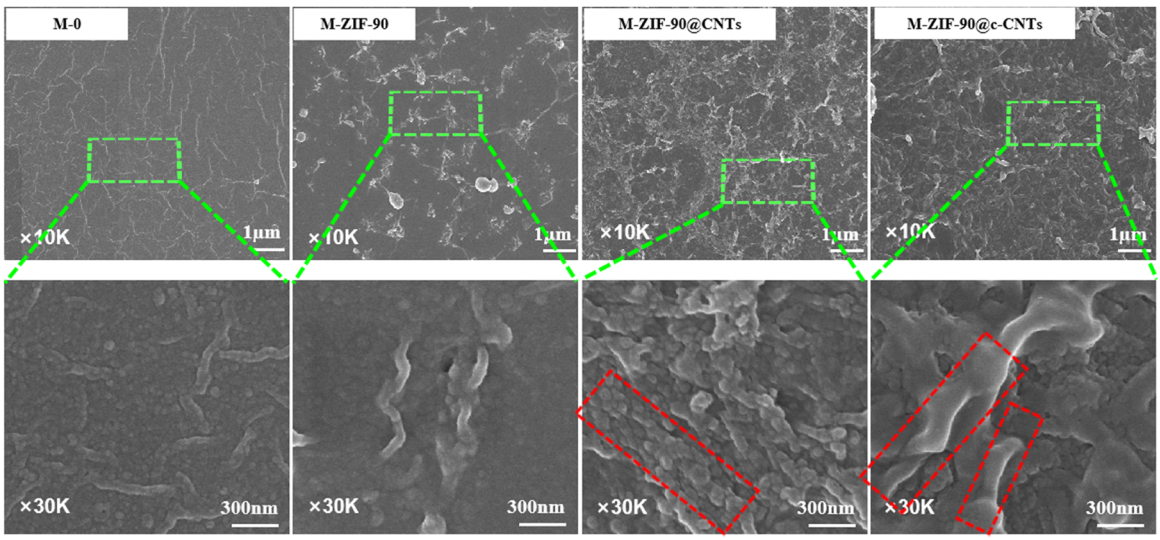

Fig. 6 SEM images of M-0, M-ZIF-90, M-ZIF-90@CNTs and M-ZIF-90@c-CNTs.

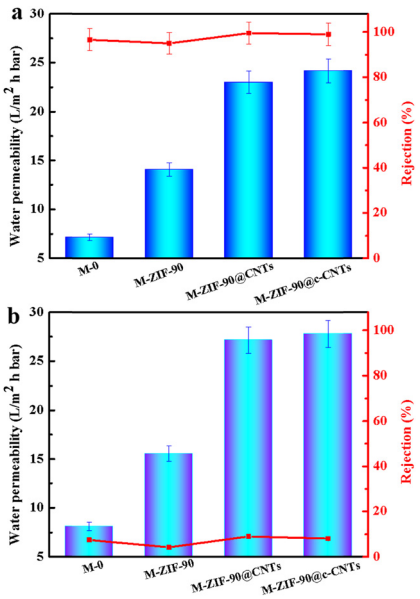

Fig. 7 (a) Dye and (b) salt rejection and water permeability of nanofiltration membranes.

membranes (M-ZIF-90, M-ZIF-90@CNTs, and M-ZIF-90@c-CNTs) were prepared by interfacial polymerization. The surface morphologies of the membranes are shown in Fig. 6. From Fig. 6, the surface of M-0 without ZIF-90 is smooth and the surface of M-ZIF-90 is uneven and obviously agglomerated. In contrast, the necklace-like M-ZIF-90@CNTs and M-ZIF-90@c-CNTs show more uniform particle dispersion. Confidently, MOF particles with precisely aligned window-to-window connections are observed, establishing micrometer-scale continuous pathways for molecular transport.

FTIR spectra of M-0, M-ZIF-90, M-ZIF-90@CNTs and M-ZIF-90@c-CNTs are shown in Fig. S7.† The FTIR spectrum of M-0 shows a absorption peak at 1669 cm^{-1}, which is C═O stretching of amide group formed by interfacial polymerization, and the characteristic band at 1582 cm^{-1} corresponds to C═O stretching of aromatic amide group. The results indicated that the polyamide layer was successfully prepared (Fig. S7a†). Furthermore, XRD analysis is shown that there is a diffraction peak at 2θ = 7.28° on M-0, M-ZIF-90@CNTs and M-ZIF-90@c-CNTs, which confirmed the presence of ZIF-90, ZIF-90@CNTs and ZIF-90@c-CNTs crystal intact in membranes, respectively (Fig. S7b†).

Congo red (CR) as a representative dye was used to test the water permeability and rejection performance of the four above types of membranes. As shown in Fig. 7a, it is clear that the water permeation of M-0 is 7.17 L m^{-2} h^{-1} bar^{-1} and the dye rejection is 96.6%. With adding ZIF-90 fillers, the water permeability of M-ZIF-90, M-ZIF-90@CNTs and M-ZIF-90@c-CNTs are increased to 14.09 L m^{-2} h^{-1} bar^{-1}, 23.02 L m^{-2} h^{-1} bar^{-1}, and 24.18 L m^{-2} h^{-1} bar^{-1}, respectively. In addition, M-ZIF-90 showed a tendency to decrease the rejection property of CR (95.02%), because ZIF-90 was agglomerated in the polymer, which resulted in a lot of interface defects between the filler and polymer.

The CR rejection of M-ZIF-90@CNTs and M-ZIF-90@c-CNTs show an increasing trend, reaching 99.55% and 99.05%, respectively. The above phenomenon may be due to the following factors: firstly, ZIF-90 has a suitable pore size, which can improve the dye rejection of the membranes. Secondly, the MOF particles in the necklace are in close contact, effectively joining the MOF window to form a relatively continuous molecular path, thus forming an ultra-high microscale continuous multi-guest molecular transport channel. Thirdly, ZIF-90@CNTs and ZIF-90@c-CNTs are uniformly distributed in the polymer and have uniform "synaptic" morphology, which can provide a larger actual surface area. The salt rejection of the prepared nanofiltration

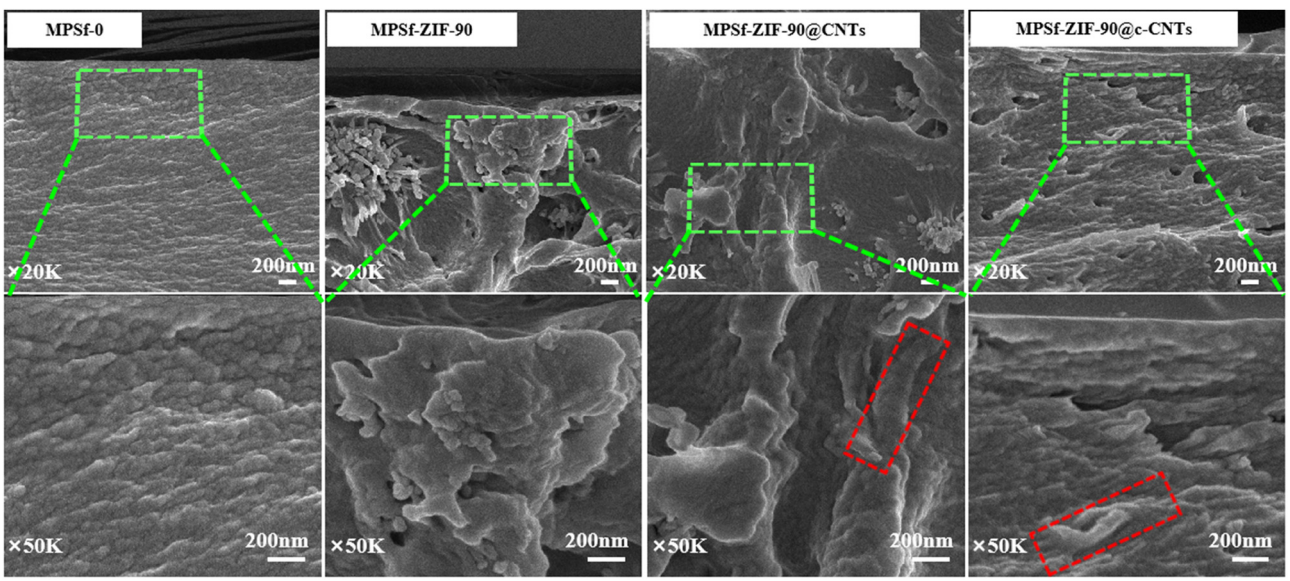

Fig. 8 The cross-sectional SEM images of MPSf-0, MPSf-ZIF-90, MPSf-ZIF-90@CNTs and MPSf-ZIF-90@c-CNTs.

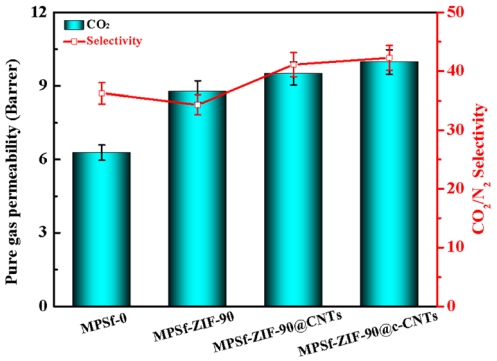

Fig. 9 Pure CO_2 permeability and ideal CO_2/N_2 selectivity of MPSf-0, MPSf-ZIF-90, MPSf-ZIF-90@CNTs and MPSf-ZIF-90@c-CNTs.

membranes are shown in Fig. 7b. The water permeation of M-ZIF-90@CNTs and M-ZIF-90@c-CNTs are 27.15 L m^{-2} h^{-1} bar^{-1}, and 27.80 L m^{-2} h^{-1} bar^{-1}, respectively and the NaCl rejection of all nanofiltration membranes is relatively low (<10%). Comparing with the representative reported nanofiltration membranes for dye/salt separation (Table S1†), the results show that M-ZIF-90@CNTs and M-ZIF-90@c-CNTs have good properties for dye/salt separation.

Furthermore, MOFs are commonly utilized as functional fillers embedded in polymer matrices for the fabrication of MMMs.[30,38,39] A self-supporting MOF/polysulfone (PSf) mixed matrix membrane was prepared by adding MOF fillers into PSf. As shown in Fig. S8,† the ZIF-90@CNTs and ZIF-90@c-CNTs fillers are uniformly distributed in the PSf matrix, but the ZIF-90/PSf MMM exhibit severe packing agglomeration and large gaps at the phase interface. Furthermore, Fig. 8 shows the cross-sectional SEM images of MPSf and modified membranes. It can be seen that ZIF-90 tends to aggregate in polymers and cannot form continuous nanochannels. Contrastively, ZIF-90@CNTs and ZIF-90@c-CNTs in the polymer can create relatively continuous molecular pathways providing potential advantages for improving molecular separation performance. The XRD patterns of MPSf-0 and modified MMMs are shown in Fig. S9.† The crystal structure

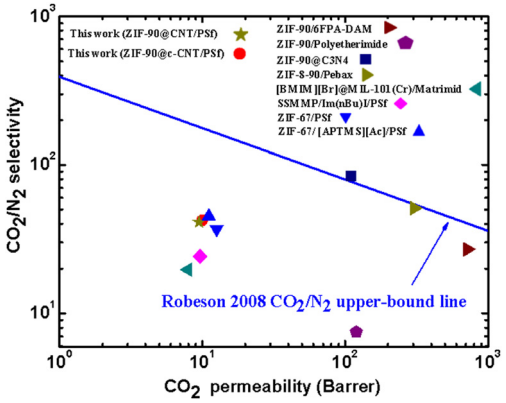

Fig. 10 CO_2/N_2 separation performances of theMPSf-ZIF-90@CNTs, MPSf-ZIF-90@c-CNTs and other MMMs in Robeson's upper bound (2008) plot.

of the ZIF-90, ZIF-90@CNTs and ZIF-90@c-CNTs are evidently maintained after being embedded into the PSf matrix, indicating a physical incorporation during the formation of the MMMs.

As shown in Fig. 9, MPSf-ZIF-90@CNTs and MPSf-ZIF-90@c-CNTs had higher pure CO_2 gas permeability and higher CO_2/N_2 ideal selectivity compared with pure PSf membranes. However, MPSf-ZIF-90 only showed high pure CO_2 permeability due to packing agglomeration. The superiority of necklace-like MOFs in a polymer matrix is also further explained. These results further demonstrate that necklace-like MOFs significantly enhance dispersion and create ultra-highly microscale continuous multi-guest molecular transport channels.

The CO_2 separation performance of the MPSf-ZIF-90@CNTs and MPSf-ZIF-90@c-CNTs are compared with that of other reported MMMs. As shown in Fig. 10 and Table S2,† ZIF-90 as a filler can significantly improve the CO_2 separation performance of mixed matrix membranes and necklace-like MOF@CNTs can enhance the separation performance of PSf membranes.

Conclusions

In summary, a simple one-pot synthesis strategy was proposed for constructing necklace-like MOF@CNTs using CNTs as the "lead wire" template. The introduction of CNTs maintains the overall framework structure and excellent stability of the original MOFs. This strategy has also been successfully applied to ZIF-8, MOF-801, UiO-66, and UiO-66-NH_2, demonstrating its universality. MOF@CNTs are dispersed uniformly in the polymer matrix, and create micrometer-scale continuous molecular transport channels that can improve the separation performance of MMMs. ZIF-90@CNTs/PA mixed matrix nanofiltration membranes exhibit higher dye rejection in dye/salt separation and ZIF-90@CNTs/PSf gas separation membranes exhibit higher CO_2 permeability and selectivity in CO_2/N_2 separation. Based on the above analysis, we have reason to believe that this work will provide a reference for the design and construction of multifunctional necklace-like MOF materials and well-dispersed-MOF based mixed matrix membranes.

Data availability

The data supporting this article have been included as part of the ESI.†

Author contributions

Xuemeng Jia: investigation, conceptualization, methodology, data management, formal analysis, writing – original draft, writing – reviewing and editing, and funding acquisition. Zhenting Song: investigation, experimentation, methodology, data management, verification, formal analysis, and writing – original draft. Qiaomei Li: investigation, verification, and supervision. Jiacheng Huang: conceptualization and

supervision. Xiaowen Zhai: investigation and supervision. Lei Tian: conceptualization, supervision, and resources. Jinlou Li: conceptualization, supervision, resources, writing – reviewing and editing. Zhihua Qiao: conceptualization, supervision, writing – review and editing, reading and final approval of the version to be published. Yuhui Luo: conceptualization, supervision, writing – review and editing, project management, reading and final approval of the version to be published. Dongen Zhang: supervision, critically reading, reading and final approval of the version to be published.

Conflicts of interest

The authors declare that they have no known competing financial interests or personal relationships.

Acknowledgements

This work was supported by PhD research startup foundation of Jiangsu Ocean University. (Grant No. KQ21034) and the China Postdoctoral Science Foundation (Certificate Number: 2024M761205).

References

1 S. M. Alardhi, N. S. Ali, N. M. C. Saady, S. Zendehboudi, I. K. Salih, J. M. Alrubaye and T. M. Albayati, *J. Ind. Eng. Chem.*, 2024, **130**, 91–104.
2 S. Li, W. Han, Q. F. An, K. T. Yong and M. J. Yin, *Adv. Funct. Mater.*, 2023, **33**, 2303447.
3 D. A. Nguyen, D. V. Nguyen, G. Jeong, N. Asghar and A. Jang, *Chem. Eng. J.*, 2023, **461**, 141789.
4 X. Sun, M. Di, J. Liu, L. Gao, X. Yan and G. He, *Small*, 2023, **19**, 2303757.
5 Y. Zhang, Z. Yuan, X. Deng, H. Wei, W. Wang, Z. Xu, Y. Feng and X. Shi, *Food Chem.*, 2022, **386**, 132753.
6 M. S. L. Tijink, J. Kooman, M. Wester, J. Sun, S. Saiful, J. A. Joles, Z. Borneman, M. Wessling and D. F. Stamatialis, *Blood Purif.*, 2014, **37**, 1–3.
7 S. H. Goh, H. S. Lau and W. F. Yong, *Small*, 2022, **18**, 2107536.
8 S. Najari, S. Saeidi, F. Gallucci and E. Drioli, *Rev. Chem. Eng.*, 2021, **37**, 363–406.
9 H. R. Harami, F. Amirkhani, H. Abedsoltan, M. Younas, M. Rezakazemi, M. Sheikh and S. Shirazian, *ChemBioEng Rev.*, 2021, **8**, 27–43.
10 L. Zhou, S. Li, L. Chen, Q. Li, C. Lu, L. Tan, L. Dong, C. Zhou and J. Cheng, *Sep. Purif. Technol.*, 2024, **330**, 125324.
11 G. Chen, C. Chen, Y. Guo, Z. Chu, Y. Pan, G. Liu, G. Liu, Y. Han, W. Jin and N. Xu, *Science*, 2023, **381**, 1350–1356.
12 M. Pakizeh, M. Karami, S. Kooshki and R. Rahimnia, *J. Taiwan Inst. Chem. Eng.*, 2023, **150**, 105025.
13 Q. Xin, J. Dong, W. Shao, X. Ding, N. Gao, L. Zhang, H. Jin, H. Chen and Y. Zhang, *J. Membr. Sci.*, 2025, **714**, 123431.
14 X. Yang, X. Chen, X. Su, A. Cavaco-Paulo, H. Wang and J. Su, *Int. J. Biol. Macromol.*, 2024, 136671.
15 C. Rizzuto, E. Tocci, E. Esposito, L. Calucci, F. Nardelli, M. Taddei, M. Lessi, F. Costantino, V. Guiotto, M. Signorile, V. Crocellà and A. Fuoco, *ACS Appl. Nano Mater.*, 2024, **7**, 23684–23695.
16 R. Lin, B. V. Hernandez, L. Ge and Z. Zhu, *J. Mater. Chem. A*, 2018, **6**, 293–312.
17 X. Jia, Z. Qiao, B. He and C. Zhong, *J. Mater. Chem. A*, 2020, **8**, 11928–11932.
18 A. Ozcan, D. Fan, S. J. Datta, A. Diaz-Marquez, R. Semino, Y. Cheng, B. Joarder, Y. Cheng and G. Maurin, *Sci. Adv.*, 2024, **10**, eadk5846.
19 L. Fei, C. Chen, L. Shen, Y. Zhang, B. Wang, J. Xu, B. Li, S. Raza and H. Lin, *Chem. Eng. J.*, 2023, **460**, 141694.
20 L. Xu, S. Li, H. Mao, A. Zhang, W. Cai, T. Wang and Z. Zhao, *J. Mater. Chem. A*, 2021, **9**, 11853–11862.
21 Q. Wang, J. Dai, W. Li, Z. Wei and J. Jiang, *Compos. Sci. Technol.*, 2008, **68**, 1644–1648.
22 P. Yu, Q. Huang, Y. Wang, W. Peng, Z. Jia, H. Wang, J. Ma, C. Wang and X. Yan, *Chin. J. Chem.*, 2024, **42**, 516–522.
23 C. Hong, Q. Li, F. Song, H. Lai, H. Xie, Y. Hao and S. Xu, *Carbon*, 2024, **228**, 119415.
24 J. Wang, M. Khan, A. Hussain, I. Khan, A. Nawaz, A. H. Ragab, A. Sayqal, T. Lei and A. Zada, *J. Mater. Res. Technol.*, 2023, **24**, 608–622.
25 K. Balasubramanian and M. Burghard, *Small*, 2005, **1**, 180–192.
26 E. M. Alosime, *Discover Nano*, 2023, **18**, 12.
27 F. Xiao, M. Cao and Y. Chen, *Desalination*, 2022, **544**, 116146.
28 N. Yang, X. Jia, D. Wang, C. Wei, Y. He, L. Chen and Y. Zhao, *J. Membr. Sci.*, 2019, **574**, 86–99.
29 Z. Zhang, X. Jia, Y. Sun, X. Guo, H. Huang and C. Zhong, *Green Chem. Eng.*, 2021, **2**, 104–110.
30 F. Gu, D. Li, R. Ding, J. Gao, X. Ruan, X. Jiang, G. He and W. Xiao, *Sep. Purif. Technol.*, 2022, **280**, 119803.
31 W. Morris, C. J. Doonan, H. Furukawa, R. Banerjee and O. M. Yaghi, *J. Am. Chem. Soc.*, 2008, **130**, 12626–12627.
32 X. Chen, N. Li, L. Chen, C. Wu and Q. Zhou, *Sep. Purif. Technol.*, 2024, **336**, 126233.
33 A. Huang, W. Dou and J. Caro, *J. Am. Chem. Soc.*, 2010, **132**, 15562–15564.
34 S. Chen, H. Pang, J. Sun and K. Li, *Mater. Chem. Front.*, 2024, **8**, 1195–1211.
35 J. Qiao and X. Li, *J. Mater. Eng. Perform.*, 2021, **49**, 27–40.
36 N. C. Burtch, H. Jasuja and K. S. Walton, *Chem. Rev.*, 2014, **114**, 10575–10612.
37 C. Wang, X. Liu, N. K. Demir, J. P. Chen and K. Li, *Chem. Soc. Rev.*, 2016, **45**, 5107–5134.
38 W. Yang, Y. Zhu, Z. Sun, C. Gao and L. Xue, *Adv. Mater. Interfaces*, 2019, **6**, 1901482.
39 X. Wang, R. Yao, H. Zhu, Z. Zhang, L. Zhang, Q. Ma, H. Jin and Y. Li, *Chem. Eng. J.*, 2024, **496**, 153737.